A Giant Electrocaloric Effect in Nanoscale Antiferroelectric and Ferroelectric Phases Coexisting in a Relaxor $Pb_{0.8}Ba_{0.2}ZrO_3$ Thin Film at Room Temperature

Biaolin Peng, Huiqing Fan, and Qi Zhang**

Recently, large electrocaloric effects (ECE) in antiferroelectric sol-gel $PbZr_{0.95}Ti_{0.05}O_3$ thin films and in ferroelectric polymer P(VDF-TrFE)55/45 thin films were observed near the ferroelectric Curie temperatures of these materials (495 K and 353 K, respectively). Here a giant ECE ($\Delta T = 45.3$ K and $\Delta S = 46.9$ J K^{-1}k g^{-1} at 598 kV cm^{-1}) is obtained in relaxor ferroelectric $Pb_{0.8}Ba_{0.2}ZrO_3$ (PBZ) thin films fabricated on Pt(111)/TiO_x/SiO_2/Sis ubstrates using a sol-gel method. Nanoscale antiferroelectric (AFE) and ferroelectric (FE) phases coexist at room temperature (290 K) rather than at the Curie temperature (408 K) of the material. The giant ECE in such a system is attributed to the coexistence of AFE and FE phases and a field-induced nanoscale AFE to FE phase transition. The giant ECE of the thin film makes this a promising material for applications in cooling systems near room temperature.

1. Introduction

The electrocaloric effect (ECE) is a change in temperature (ΔT) in a polarable material by virtue of the change in entropy (ΔS) upon the application of or withdrawing of an electric field under adiabatic conditions.[1–3] Simulation results[4] indicate that cooling devices based on a large ECE can have much higher coefficients of performance (COPs) (>60% of the Carnot efficient) than those of mechanical vapor compression cycle cooling devices such as refrigerators and air conditioners, which generate strong greenhouse gases during their operation. The bottleneck for the development of ECE cooling technologies in the past has been that only small ΔT and ΔS can be induced in bulk materials, for example only $\Delta T = 2.5$ K and $\Delta S = 0.2$ J K^{-1} kg^{-1} at 750 V in $Pb_{0.99}Nb_{0.02}(Zr_{0.75}Sn_{0.20}Ti_{0.05})O_3$ ceramics,[5] because of the restriction of breakdown fields (≈50 kV cm^{-1}).

Recently, by using a thin-film geometry, a giant ECE ($\Delta T = 12$ K and $\Delta S = 8$ J K^{-1} kg^{-1} at 776 kV cm^{-1}) in the antiferroelectric $PbZr_{0.95}Ti_{0.05}O_3$ (PZT) was observed by Mischenko et al.[1] near the antiferroelectric to paraelectric phase transition temperature (T_c = 500 K). This has triggered new interest in the search for new ECE materials, which has resulted in significant progress in this field and has raised hopes for successful development of ECE solid-state cooling units. For example, Saranaya et al.[6] reported a bigger ECE temperature change (ΔT = 31 K) at 413 K and 747 kV cm^{-1} in $Pb(Mg_{1/3}Nb_{2/3})_{0.65}Ti_{0.35}O_3$ thin films deposited by pulsed laser deposition (PLD). However, the application of a cooling devices requires a maximum EC effect at or near room temperature. In view of this, Neese et al.[3] reported a ECE temperature change (ΔT) of ≈12.6 K at 2090 kV cm^{-1} in the ferroelectric polymer poly(vinylidene fluoride-trifluoroethylene) [P(VDF-TrFE)] (55/45 mol%) thin film, near room temperature (353 K).

A large ECE can often be obtained near the Curie temperature (T_C) of ferroelectrics,[1] where the polarization (P) changes with temperature. Through the first-principles-based simulation, Ponomareva et al.[7] found that ferroelectrics with multiple transitions can exhibit a giant ECE under large electric fields and the coexistence of both positive and negative ECE in one material. Moreover, the origin of a negative ECE can be traced to the non-collinearity between the electric field and the polarization, which could induce new ways to enhance the electrocaloric efficiency.

In this work, we report a giant ECE (ΔT = 45.3 K and $\Delta S = 46.9$ J K^{-1} kg^{-1} at 598 kV cm^{-1}) in nanoscale orthorhombic antiferroelectric phases and rhombohedral ferroelectric phases coexisting in relaxor $Pb_{0.8}Ba_{0.2}ZrO_3$ thin films prepared by sol-gel method at room temperature (290 K) away from its Curie temperature (408 K). A new mechanism is introduced to interpret the dramatic ECE.

2. Results and Discussion

2.1. Structure

X-ray diffraction (XRD) patterns of PBZ thin films fabricated on a Pt(111)/TiO_x/SiO_2/Si substrate using a sol-gel method are illustrated in **Figure 1**a. Pure and good existence of

B. Peng, Prof. H. Fan
State Key Laboratory of Solidification Processing
School of Materials Science and Engineering
Northwestern Polytechnical University
Xi'an 710072, China
E-mail: hqfan3@163.com
B. Peng, Dr. Q. Zhang
Department of Manufacturing and Materials
Cranfield University
Cranfield, Bedfordshire, MK43 0AL, UK
E-mail: q.zhang@cranfield.ac.uk

DOI:10. 1002/adfm.201202525

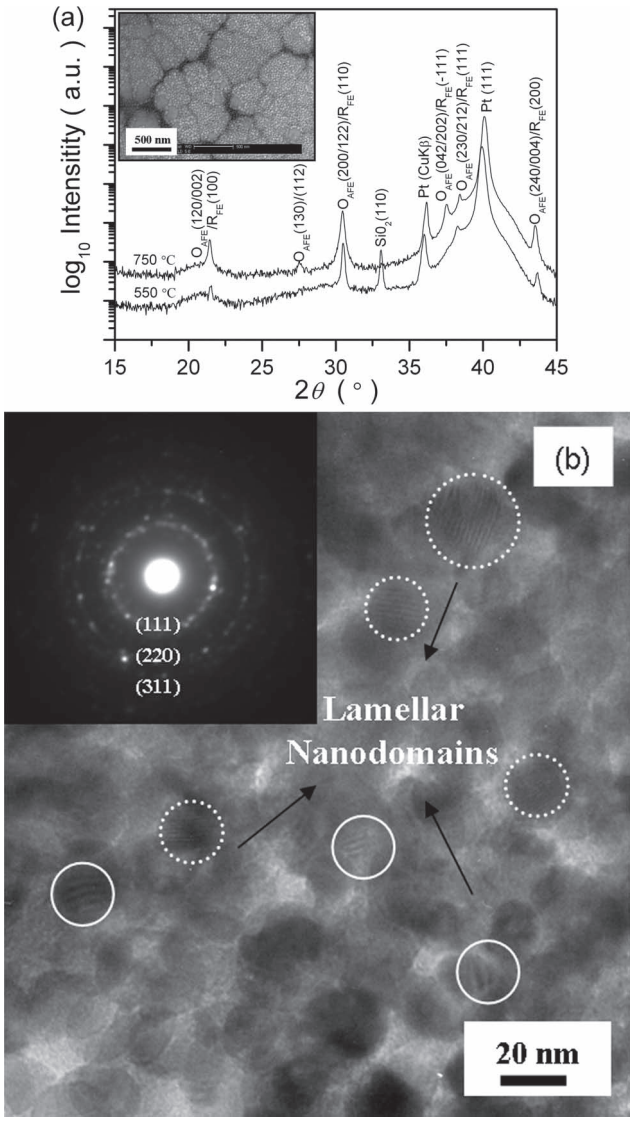

Figure 1. a) XRD patterns and SEM surface image (inset) of the PBZ thin film. b) TEM image and SAED pattern (inset).

orthorhombic antiferroelectric phase[8] in the PBZ thin film. Refined lattice parameters for the orthorhombic antiferroelectric (O_{AFE}) phase are determined to be a_O = 5.83612 Å, b_O = 11.72206 Å and c_O = 8.31065 Å using the software JADE (JADE V 7.5.1 XRD, Pattern Processing Identification & Quantification, Materials Data Inc. 2005). In addition to the O_{AFE} phase, a rhombohedral ferroelectric (R_{FE}) phase with lattice parameters a_R = 4.12267 Å and α_R = 90.9541° can also be detected. The scanning electron microscopy (SEM) surface image (inset of Figure 1a) of the PBZ thin film displays a typical rosette structure,[9] which is formed by the lead loss during the heat-treatment process[10,11] and consists of round lighted-colored regions (rosettes) and a dark region between the rosettes. Inside and in between the rosettes, subgrains with average size of 20 nm can also be clearly observed.

To further study the morphology and microstructure of PBZ thin film, transmission electron microscopy (TEM) characterization was carried out. Numerous dispersed nanocrystals corresponding to the subgrains in the SEM were observed in the TEM bright field image (Figure 1b). In the inside of some nanocrystals, lamellar nanodomains about 2 nm wide (white solid circles) and lamellar nanodomains about 1 nm wide (white dotted circles) are clearly visible. The latter can be attributed to be the antiferroelectric domains for 1 nm wide, close to its cell parameters, which is consistent with the report by Viehland[12] in PZT. Inset of Figure 1b shows the selected-area electron diffraction (SAED) pattern of the PBZ thin film. For simplicity, the lattice indices for SAED are labeled as the pseudo-cubic structure rather than the orthorhombic or rhombohedral structure. Circular rings correspond to the (111), (220), and (311) plane reflections, from inside to outside, respectively. The discontinuity of diffraction rings indirectly reveals the nanocrystalline characteristics of PBZ thin film.[13] It is well-known that the polarization vector for the R_{FE} phase is <111>[14] and the rotation between neighboring domains depends on the cell angle α. For PZT,[14] the rhombohedral angle α is 91°, and the possible types of domain can be calculated as 109°, 71°, and 180°. The orientation of permissible uncharged walls is {110} for 109°, {001} for 71° and the plane parellel to the polarization vector is 180° domain. According to the refined α value (90.9541°) of the R_{FE} phase and the feature of the SAED pattern of PBZ thin film, lamellar nanodomains with about 2 nm wide probably is due to the exisitence of 180° ferroelectric domains, which need to be further confirmed using piezoresponse force microscopy (PFM).

2.2. Dielectric Properties

Temperature dependences of dielectric permittivity (ε) and dielectric loss (tan δ) at different frequencies are shown in **Figure 2**a. Although the dielectric permittivity is higher ($\varepsilon_m \approx$ 1200) compared with that found in PZT-based compositions, it is rather lower than obtained for corresponding sintered bulk PBZ ceramics with the same composition ($\varepsilon_m \approx$ 12 000).[15,16] This difference can be attributed to the small grain size in thin films, in contrast to with similar bulk ceramics, and due to substrate constraint.[17–21] Likewise, the maximum dielectric permittivity is observed at 408 K (T_m), rather than at 425 K as reported in PBZ bulk material.[15,16] The relaxation observed by the frequency dependence of the dielectric permittivity indicates the existence of defects (small thickness of the film, clamping by the substrate and low annealing temperature), which may contribute to decreasing of permittivity and the shift in T_m compared to bulk ceramics. Moreover, the antiferroelectric to ferroelectric (AFE–FE) transition cannot be detected in the whole temperature range, which is similar to the phenomenon in PZT thin film.[1]

In order to evaluate the ECE in the PBZ thin film, the electric field dependence of the polarization (*P*–*E*) loops at 100 Hz were measured at a 5 K interval in the temperature range between 283 K and 418 K. Representative plots of *P*–*E* loops are shown in Figure 2b,c. The temperature dependence of the polarization ($P(T)$) at selected electric field values, established from the upper branches of the *P*-*E* hysteresis loops in $E > 0$, is presented in the insets of Figure 2b,c. The solid lines in the

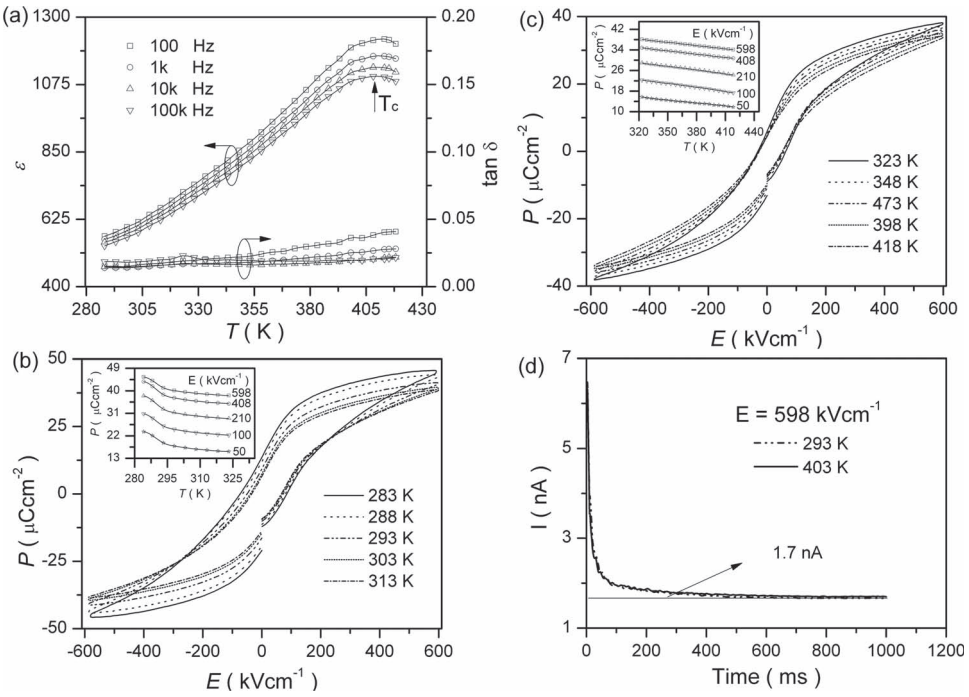

Figure 2. a) $\varepsilon(T)$ and tan $\delta(T)$ of PBZ thin film. b,c) *P*–*E* loops at selected temperatures, the inset shows $P(T)$ at selected electric field values. d) Leakage current $I(t)$.

inset of Figure 2b,c represent cubic-spline interpolations of the raw data.

Leakage currents ($I(t)$) measured in the maximum field employed (598 kV cm^{-1}) (Figure 2d) were investigated at room temperature 293 K and near the Curie temperature, 403 K, respectively. The observed transients persist up to 1000 ms, even beyond which no breakdown occurs after repetitive testing. By contrast, beyond 200 ms breakdown occurs in the PZT thin film.[1] It can be seen that 1.7 nA is an upper bound for the steady-state leakage current. This value yields negligible Joule heating (<10^{-3} K) and does not affect $P(E)$ because currents of hundreds of μA are required to switch the measured polarizations at 100 Hz.

2.3. Electrocaloric Effect

Reversible adiabatic changes in temperature (ΔT) and entropy (ΔS) for a material of density (ρ) with heat capacity (C) are given[1–3,22,23] by

$$\Delta T = -\frac{1}{\rho}\int_{E1}^{E2}\frac{T}{c}\left(\frac{\partial P}{\partial T}\right)\mathrm{d}E \quad (1)$$

$$\Delta S = -\frac{1}{\rho}\int_{E1}^{E2}\left(\frac{\partial P}{\partial T}\right)\mathrm{d}E \quad (2)$$

assuming the Maxwell relation $(\partial P/\partial T)_E = (\partial S/\partial E)_T$. Values of $(\partial P/\partial T)_E$ were obtained from fourth-order polynomial fits to the cubic-spline interpolation of raw $P(T)$ data extracted from the upper branches of *P*–*E* loops in $E > 0$ (see the inset of Figure 2b,c). In the temperature range of interest, the heat capacity (C = 330 J K^{-1} kg^{-1}) remains constant for Zr-rich lead-based thin films, and the peak associated with the transition is <10% of the background.[1] Assuming a constant value of C despite an ≈50% peak[1] resulted in excellent agreement with direct ECE measurements of ΔT in bulk $Pb_{0.99}Nb_{0.02}(Zr_{0.75}Sn_{0.20}Ti_{0.05})_{0.98}O_3$. Therefore, C = 330 J K^{-1} kg^{-1} can be taken as the heat capacity value of the PBZ thin film. The theoretical density ρ of PBZ thin film with the pseudocubic structure can be determined to be 7.7 g cm^{-3} by using the software JADE. Using Equation (1) and (2), ΔT and ΔS at selected electric fields are shown in **Figure 3**a,b and in the insets of Figure 3a,b, respectively. Peak ΔT = 45.3 °C at 598 kV cm^{-1} was obtained at 290 K (see Figure 3a), as well as peak ΔS = 46.9 J K^{-1} kg^{-1} (see inset of Figure 3a).

For comparison, **Table 1** lists the ECE characteristics of PBZ, $PbZr_{0.95}Ti_{0.05}O_3$,[1] P(VDF-TrFE)55/45,[2,3] $PbSc_{0.5}Ta_{0.5}O_3$,[24] PMN-PT90/10,[23] and $Pb(Mg_{1/3}Nb_{2/3})_{0.65}Ti_{0.35}O_3$ thin films.[6] The ΔT, $\Delta T/\Delta E$ and $\Delta T\Delta S$ of the PBZ thin film are the largest among all of them, except the ΔS (60 J K^{-1} kg^{-1} for P(VDF-TrFE)55/45). The large $\Delta T\Delta S$ value (2125 J kg^{-1}) of the PBZ thin film at room temperature means a large refrigerant capacity (RC), which is required in cooling systems. Moreover, the peak ΔT = 45.3 K at 598 kV cm^{-1}, represents a peak energy change $C\Delta T$ = 14.95 kJ kg^{-1}, and the corresponding hysteresis loss taken near the peak (T_{ECE} = 293 K) was about 5.5% of the energy change. Hysteresis losses have the potential to reduce the peak ECE temperature change by only 2.5 K. Hysteresis losses may be reduced[25] by i) reducing the measurement

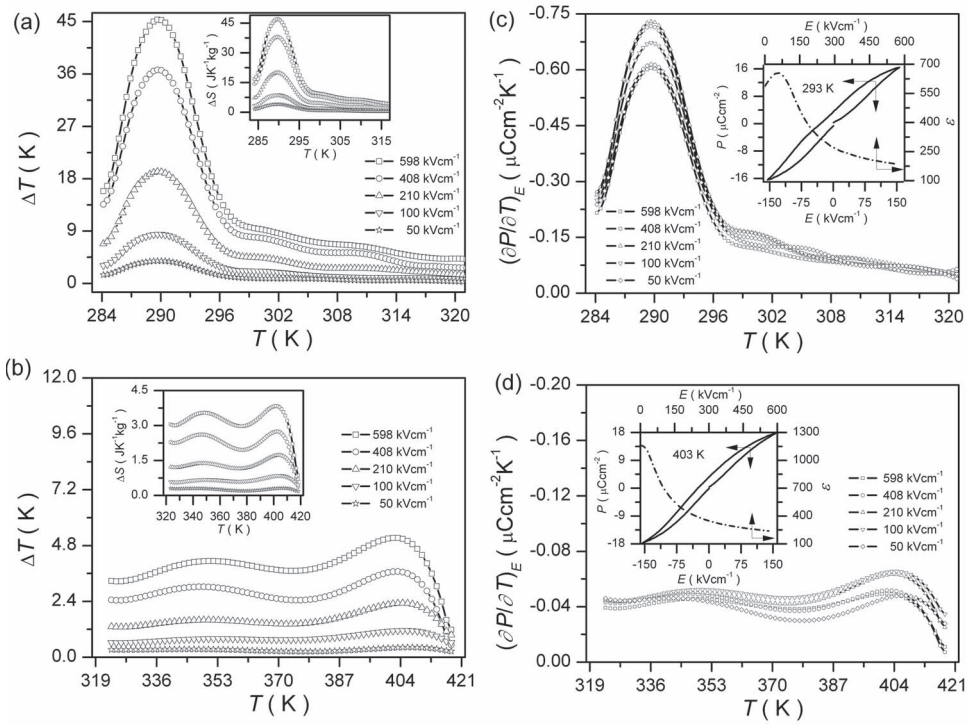

Figure 3. a,b) ΔT of PBZ film at selected electric fields, the inset is ΔS. c,d) $(\partial P/\partial T)_E$ of PBZ films at selected electric fields. The inset shows the P–E loop and $\varepsilon(E)$ measured at 293 K and 403 K.

frequency, ii) introducing chemical substituents, and iii) modifying microstructures.

Twin-peak ECEs with a maximum $\Delta T < 5$ °C (Figure 3b) and $\Delta S < 4.5$ J K^{-1} kg^{-1} (inset of Figure 3b) were observed. Such twin-peak ECE also have been reported in several perovskite relaxors.[26–29] The appearance of the twin peak can be explained with the field-induced polar nanodomain formation and alignment of these polar species.[30] The low-temperature peak and the high-temperature peak of the twin peaks correspond to the depolarization temperature (T_{dp}) and the Curie temperature,[31,32] respectively.

In order to elucidate the giant ECE in PBZ thin film, the pyroelectric coefficients $(\partial P/\partial T)_E$ at selected electric fields are plotted in Figure 3c,d. It is clear from Figure 3c that with the increase of the electric field, the $(\partial P/\partial T)_E$ around the temperature of the peak first increases and reaches a maximum at 210 kV cm^{-1}, and then decreases. Likewise, in Figure 3d, the $(\partial P/\partial T)_E$ near and between the temperature of the twin-peak first increases and reaches a maximum at 100 kV cm^{-1}, and then decreases.

To obtain insight into this phenomenon, P–E loops under different electric fields and the dc electric field dependence of the permittivity ($\varepsilon(E)$) were investigated at 293 K and 403 K. Double P–E loops were visible at 293 K when the electric field is lower than 210 kVcm^{-1}, as shown in the inset of Figure 3c, indicating that an electric field induced AFE–FE phase transition occurs.[33,34] Typical ferroelectric P–E loops were obtained when the electric field was higher than 210 kV cm^{-1}, as shown in Figure 2b. In contrast, only ferroelectric P–E loops can be obtained at 403 K under all electric fields, as shown in the inset of Figure 3d. A peak in the curve of $\varepsilon(E)$ (inset of Figure 3c) was observed at 293 K, which further revealed the existence of the electric field induced AFE–FE phase transition.[33,34] No peak can be detected in the curve of $\varepsilon(E)$ (inset of Figure 3d) at 403 K.

Table 1. Electrocaloric characteristics of thin films.

Material	T [°C]	ΔT [°C]	ΔE [kV cm^{-1}]	$\Delta T/\Delta E$ [K cm kV^{-1}]	ΔS [J K^{-1}k g^{-1}]	$\Delta T\Delta S$ [J kg^{-1}]
$Pb_{80}Ba_{20}ZrO_3$	17	45.3	598	0.076	46.9	2125
$PbZr_{0.95}Ti_{0.05}O_3$[1]	222	12	776	0.015	8	96
P(VDF-TrFE)55/45[2,3]	80	12.6	2090	0.006	60	756
$PbSc_{0.5}Ta_{0.5}O_3$[24]	68	6.2	774	0.008	6.3	39
PMN-PT90/10[23]	75	5	895	0.006	5.6	28
$Pb(Mg_{1/3}Nb_{2/3})_{0.65}Ti_{0.35}O_3$[6]	140	31	747	0.041	32	992

From the above analysis, it can be inferred that the giant EC at room temperature for PBZ thin film may be caused by the electric field-induced AFE–FE phase transition, which could induce new ways to enhance the electrocaloric efficiency by virtue of the noncollinearity between the electric field and the polarization.[7] It is well-known that for second order phase transitions or higher order phase transitions, the entropy change ΔS is usually normally smaller than fthe irst order phase transition. Bhadra et al.[8] carried out a high temperature X-ray study of structure phase transitions in $Pb_{1-x}Ba_xZrO_3$ powders and confirmed the first order nature of the A_O to F_R transition. The A_O to F_R transition is similar to the austensite (A) to martensite (M) transition[8] in some alloys, and large ΔS can be caused during the transition. Previous work[31,32] pointed out that latent heat (or ΔS) from the field-induced phase transition can significantly contribute to the ECE below the depolarization temperature T_{dp}. Therefore, the giant ECE at room temperature for PBZ thin films can be attributed to the contribution of the electric field induced A_O to F_R transition. However, the transition of AFE to FE phases may not be the only phenomenon responsible for the large ECE in the PBZ system. Orientation of nanoregions existing in the thin film under an electric field may also contribute to the giant ECE because a large entropy change from totally random nanoregions to ordered nanoregions occurs. The effect of orientation of the nanoregions induced by the electric field on the ECE is under investigation.

Moreover, the latest work of Zhang et al.[35] showed that a large ECE can be obtained in materials with an invariant critical point (ICP), where multiphase coexistance and large entropy change ΔS can be obtained during the phase transition. As a relaxor with the structure of nano-scaled O_{AF} phase and R_F phase coexist, the PBZ thin film with giant ECE at room temperature can be assumed to be a material with an ICP. For this, further theoretical research is needed.

3. Conclusions

A giant ECE (ΔT = 45.3 K and ΔS = 46.9 J K^{-1} kg^{-1} at 598 kV cm^{-1}) at room temperature (290 K) rather than at the Curie temperature (408 K) was obtained in the antiferroelectric and ferroelectric phases coexisting in relaxor $Pb_{0.8}Ba_{0.2}ZrO_3$ thin films fabricated on Pt(111)/TiO_x/SiO_2/Si substrates using a sol-gel method. Field-induced nanoscale antiferroelectric to ferroelectric phase transitions play a key role in the dramatic EC effect. The PBZ thin film can possibly be used for applications in cooling systems near room temperature.

4. Experimental Section

Fabrication: $Pb_{80}Ba_{20}ZrO_3$ (PBZ) thin films were fabricated by a sol-gel method. $Pb(OAc)_2{\cdot}3H_2O$ and $Ba(OAc)_2$ were dissolved in glacial acetic acid and deionized water. In order to compensate for the Pb loss during sintering, 20% excess Pb was added. Separately, acetylacetone was added to a mixture of $Zr(O^nPr)_4$ and 2-methoxyethanol and the resulting solution was stirred at room temperature for 30 min. The Pb/Ba and Zr solutions were mixed and stirred at room temperature for 2 h. The final concentration of the synthesized PBZ sol was 0.3 M. After aging the sol for 24 h. PBZ sols were passed through a 0.2 μm filter for spin coating at 4000 rpm for 30 s onto Pt(111)/TiO_x/SiO_2/Si(100) substrates that were rinsed with acetone and 1-propanol. Each layer was pyrolized at 350 °C for 3 min and then heated at 550 °C for 5 min on hotplates. After the deposition of 8 layers, the film was annealed in a tube furnace at 750 °C for 30 min in air. The final thickness of the film was about 320 nm. Cr/Au top electrodes of 150 μm diameter were deposited by thermal evaporation.

Characterization: The PBZ film structure was monitored by XRD (Bruker-AXS D5005, Siemens, Munich, Germany) on a diffractometer, using Cu Kα radiation (λ = 1.5406 Å). The surface morphology of the film was examined using SEM (FEI XL30 SFEG, Philips, Edihoven, The Netherlands). The microstructure of the film was studied by TEM (CM20, Philips, Edihoven, The Netherlands). Dielectric permittivity measurements were carried out using an impedance analyzer (Wayne-Kerr Electronics, UK) at V = 100 mV. Electric dependences of polarization hysteresis (*P-E*) loop and leakage current (*I–E*) were obtained by means of a ferroelectric tester (RT66A, Radiant Technologies Inc., Albuquerque, NM, USA). Temperature was controlled with the aid of a Peltier element.

Acknowledgements

B.P. would like to thank the National Natural Science Foundation (51172187), the SPDRF (20116102130002), 111 Program (B08040) of MOE, the Xi'an Science and Technology Foundation (CX1261-2, CX1261-3) of China, and China Scholarship Council for personel financial support for working in Cranfield.

Received: September 3, 2012
Revised: October 30, 2012
Published online: January 20, 2013

[1] A. S. Mischenko, Q. Zhang, J. F. Scott, R. W. Whatmore, N. D. Mathur, *Science* **2006**, *311*, 1270.
[2] S.-G. Lu, Q. Zhang, *Adv. Mater.* **2009**, *21*, 1983.
[3] B. Neese, B. Chu, S.-G. Lu, Y. Wang, E. Furman, Q. M. Zhang, *Science* **2008**, *321*, 821.
[4] O. V. Pakhomov, S. F. Karamenko, A. A. Semenov, A. S. Starkov, A. V. Es'kov, *Tech. Phys.* **2010**, *55*, 1155.
[5] B. A. Tuttle, D. A. Payne, *Ferroelectrics* **1981**, *37*, 603.
[6] D. Saranya, A. R. Chaudhuri, J. Parui, S. B. Krupanidhi, *Bull. Mater. Sci.* **2009**, *32*, 259.
[7] I. Ponomareva, S. Lisenkov, *Phys. Rev. Lett.* **2012**, *108*, 167604.
[8] B. P. Pokharel, D. Pandey, *J. Appl. Phys.* **2001**, *90*, 2985.
[9] L. Pintilie, I. Boerasu, M. J. M. Gomes, M. Pereira, *Thin Solid Films* **2004**, *458*, 114.
[10] X. Hao, J. Zhai, X. Chou, X. Yao, *Solid State Commun.* **2007**, *142*, 498.
[11] E. M. Alkoy, S. Alkoy, T. Shiosaki, *Japan J. Appl. Phys.* **2005**, *44*, 6654.
[12] D. Viehland, *Phys. Rev. B* **1995**, *52*, 778.
[13] S. Singh, S. B. Krupanidhi, *J. Appl. Phys.* **2012**, *111*, 024314.
[14] J. Ricote, R. W. Whatmore, D. J. Barber, *J. Phys.: Condens. Matter* **2000**, *12*, 323.
[15] B. P. Pokharel, D. Pandey, *J. Appl. Phys.* **2000**, *88*, 5364.
[16] B. P. Pokharel, D. Pandey, V. Siruguri, S. K. Paranjpe, *Appl. Phys. Lett.* **1999**, *74*, 756.
[17] N. A. Pertsev, A. G. Zembilgotov, A. K. Tagantsev, *Phys. Rev. Lett.* **1998**, *80*, 1988.
[18] S. P. Alpay, I. B. Misirlioglu, A. Sharma, Z.-G. Ban, *J. Appl. Phys.* **2004**, *95*, 8118.
[19] G. Akcay, S. P. Alpay, J. V. Mantese, G. A. Rossetti, *Appl. Phys. Lett.* **2007**, *90*, 252909.

[20] J. Zhang, S. P. Alpay, G. A. Rossetti, *Appl. Phys. Lett.* **2011**, *98*, 132907.
[21] G. Akcay, S. P. Alpay, G. A. Rossetti, J. F. Scott, *J. Appl. Phys.* **2008**, *103*, 024104.
[22] T. M. Correia, J. S. Young, R. W. Whatmore, J. F. Scott, N. D. Mathur, Q. Zhang, *Appl. Phys. Lett.* **2009**, *95*, 182904.
[23] A. S. Mischenko, Q. Zhang, R. W. Whatmore, J. F. Scott, N. D. Mathur, *Appl. Phys. Lett.* **2006**, *89*, 242912.
[24] T. M. Correia, S. Kar-Narayan, J. S. Young, J. F. Scott, N. D. Mathur, R. W. Whatmore, Q. Zhang, *J. Phys. D: Appl. Phys.* **2011**, *44*, 165407.
[25] D. Viehland, J. F. Li, *J. Appl. Phys.* **2011**, *89*, 1826.
[26] J. Hagberg, A. Uusimäki, H. Jantunen, *Appl. Phys. Lett.* **2008**, *92*, 132909.
[27] J. Peräntie, J. Hagberg, A. Uusimäki, H. Jantunen, *Phys. Rev. B* **2010**, *82*, 134119.
[28] M. Valant, L. J. Dunne, A.-K. Axelsson, N. McN. Alford, G. Manos, J. Peräntie, J. Hagberg, H. Jantunen, A. Dabkowski, *Phys. Rev. B* **2010**, *81*, 214110.
[29] L. Shebanovs, K. Borman, W. N. Lawless, A. Kalvane, *Ferroelectrics* **2002**, *273*, 137.
[30] L. J. Dunne, M. Valant, A. K. Axelsson, G. Manos, N. M. Alford, *J Phys D: Appl. Phys.* **2011**, *44*, 375404.
[31] G. C. Lin, X. M. Xiong, J. X. Zhang, Q. Wei, *J. Therm. Anal. Calorim.* **2005**, *81*, 41.
[32] G. Sebald, S. Pruvost, L. Seveyrat, L. Lebrun, D. Guyomar, B. Guiffard, *J. Eur. Ceram. Soc.* **2007**, *27*, 4021.
[33] Y. Liu, X. Lu, Y. Jin, S. Peng, F. Huang, Y. Kan, T. Xu, K. Min, J. Zhu, *Appl. Phys. Lett.* **2012**, *100*, 212902.
[34] T. M. Correia, Q. Zhang, *J. Appl. Phys.* **2010**, *108*, 044107.
[35] Z. K. Liu, Xinyu Li, Q. M. Zhang, *Appl. Phys. Lett.* **2012**, *101*, 082904.